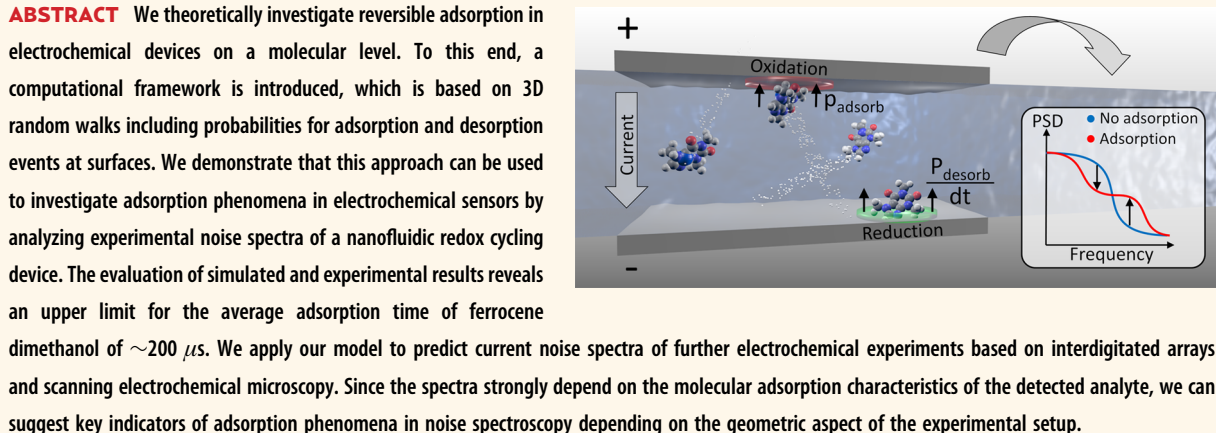


Noise Phenomena Caused by Reversible Adsorption in Nanoscale Electrochemical Devices

Enno Kätelhön,^{†,‡} Kay J. Krause,[†] Klaus Mathwig,[‡] Serge G. Lemay,[‡] and Bernhard Wolfrum^{†,§,*}

[†]Institute of Bioelectronics (PGI-8/ICS-8) and JARA—Fundamentals of Future Information Technology, Forschungszentrum Jülich, 52425 Jülich, Germany,

[‡]MESA+ Institute for Nanotechnology, University of Twente, PO Box 217, 7500 AE Enschede, The Netherlands, and [§]Institute of Physics, RWTH Aachen University, 52074 Aachen, Germany. [‡]Present address: Department of Chemistry, Physical and Theoretical Chemistry Laboratory, University of Oxford, South Parks Road, Oxford OX1 3QZ, United Kingdom.



KEYWORDS: nanoelectrochemistry · noise spectroscopy · adsorption spectroscopy · redox cycling · nanofluidics

Adsorption phenomena may impact the performance of electrochemical devices in multiple ways and play a crucial role in the development of nanoscale sensors. Particularly, the reversible or permanent adsorption of analyte molecules at sensing electrodes turns out to be of increasing importance at small scales, where analyte transport toward the electrode is accelerated through spherical diffusion profiles. The same applies to experiments involving repeated analyte reactions in fast-scan voltammetry^{1,2} or redox cycling. In the latter case, similar to nanoelectrode experiments, the analyte mass transfer toward the electrode is enhanced, enabling significantly higher reaction rates in diffusion-limited processes as well as an increased impact of adsorption effects. In redox cycling devices the ratio between electrode surface and enclosed volume is typically very high ($>10^7 \text{ m}^{-1}$), representing a good system for the investigation of adsorption phenomena. Such devices can be

implemented in a variety of designs,^{3,4} but always comprise two individually biased electrodes that are located in close proximity to each other. Analyte molecules can diffuse between the electrodes and undergo repeated redox reactions, thus establishing a current across the gap. Due to the increased mass transfer to the electrodes, this effect leads to a significant amplification of the Faradaic current and represents the central advantage of this approach.

Most reported experiments utilize the redox cycling effect in two experimental configurations, namely, scanning electrochemical microscopes (SECMs) and interdigitated electrodes (IDEs). In SECMs, an ultramicroelectrode typically scans across a separately biased sample surface.^{5,6} This approach is widely established today and applied in a variety of different fields of research.^{7–10} IDEs, on the other hand, feature two comb-shaped electrodes that are arranged in an interdigitated fashion on a substrate surface.^{11–14} Due to their

* Address correspondence to b.wolfrum@fz-juelich.de.

Received for review February 17, 2014 and accepted April 2, 2014.

Published online April 02, 2014
10.1021/nn500941g

© 2014 American Chemical Society

comparably simple fabrication and easy lab-on-a-chip integration, IDEs are now used in a wide range of applications.^{15–18} Other on-chip approaches include pore-based sensors^{19–24} that are formed through an interpenetrated electrode stack. Additionally, precisely overlapping electrode faces can be implemented in nanofluidic or nanocavity sensors by removing a sacrificial layer between two closely spaced electrodes.^{25,26} Such devices will be addressed first in this paper.

Even though redox cycling sensors are widely used, there are only a few publications that focus on their noise characteristics. Most of these studies investigate the fluctuation of the Faradaic current or the stochastic sensing of single molecules in either SECM experiments^{27,28} or nanofluidic devices.^{29–31} In previous studies we analyze the origin of different types of noise that can be found in the current response of nanofluidic sensors.^{32–34} Here, we expand recent work on the simulation of noise phenomena³⁴ by investigating the impact of molecular adsorption on the noise spectra of redox cycling sensors. We first show that our simulation model reproduces theoretical expectations in simple geometries. We then take a further step and simulate the spectrum of a realistic nanofluidic electrochemical sensor. We compare the experimental data with simulated spectra and find a close match of the results. The analysis yields an upper boundary for the average adsorption times of redox-active molecules. In the last part of this work, we apply our model to more complex geometries that cannot be easily solved analytically. We predict the noise spectra of adsorbing interdigitated arrays as well as of an absorbing scanning electrochemical microscope tip near a biased conducting surface. Our simulations reveal new applications in noise spectroscopy predicting discrete boundaries for observing adsorption times.

THEORY

In former studies, three origins of current noise have been described for nanofluidic redox cycling sensors. These are namely number fluctuation noise, adsorption noise, and shot-like redox cycling noise. In the following, we will shortly discuss their nature and set our adsorption model in relation to the current state of research.

Number Fluctuation Noise. Number fluctuation noise results from active molecules that diffusively enter and leave the sensor. The change in number of molecules inside the sensor then also leads to fluctuations in the number of molecules that participate in redox cycling and causes a certain type of noise in the low-frequency regime that can be described analytically.^{32,39} For the case of adsorbing electrodes, an effective diffusion constant (D_{eff}) can be assumed inside the channel that reduces the frequency of the fluctuation noise, while preserving the spectrum's shape.^{32,33} D_{eff} can hereby be determined either from the variance of a current

trace or through a spectral analysis and turns out to be a convenient measure to determine the ratio between average adsorbed and desorbed times. This behavior can also be observed in our simulation approach. Due to adsorption at electrodes, the diffusion constant along the nanochannel is effectively lowered, since molecules reversibly adsorb after an average free time while diffusion is halted. The effective diffusion constant between the electrodes of a nanofluidic sensor is then given by

$$D_{\text{eff}} = D \frac{1}{1 + \frac{\tau_a}{\tau_d}} \quad (1)$$

where τ_d and τ_a represent the average time a molecule diffuses freely and spends adsorbed, respectively.³² However, the effective diffusion constant in our model is not assumed to be homogeneous but may vary inside the nanochannel. It depends on whether the molecule is enclosed between two electrodes, one electrode and a nonconducting surface, or two nonconducting surfaces and the device geometry. Our model can therefore be used for arbitrary designs without the need of defining area-specific diffusion constants.

Adsorption Noise. In contrast to fluctuation noise, adsorption noise impacts the number of molecules participating in redox cycling through reversible adsorption at the electrodes. Analytically, this process can be described through a two-state Markov process,³² in which molecules either participate in redox cycling and contribute a certain current to the overall sensor current or are adsorbed. In the case of an ideal nanofluidic channel, this model is fully captured by our simulation. Therefore, analytical findings can then be directly transferred to verify our simulation approach.

Shot-like Redox Cycling Noise. Shot-like redox cycling noise is caused by the Brownian motion of active molecules in between the electrodes and depends solely on the average number of free molecules inside the sensor and the interelectrode distance in the case of nonadsorbing electrodes.³⁴ It features a white noise spectrum³⁴ and is typically smaller than the formerly mentioned sources of noise in the low-frequency regime.

RESULTS

Adsorption Noise. In order to first study adsorption noise isolated from number fluctuation noise, we start our investigations using a simple redox cycling system that solely consists of two infinite parallel electrodes, as shown in Figure 1a. Here the number of molecules between the electrodes remains constant throughout the simulation. The resulting current is therefore affected only by adsorption noise and shot-like redox cycling noise.

Figure 1b presents the simulated power spectral densities in comparison to the analytical solution.

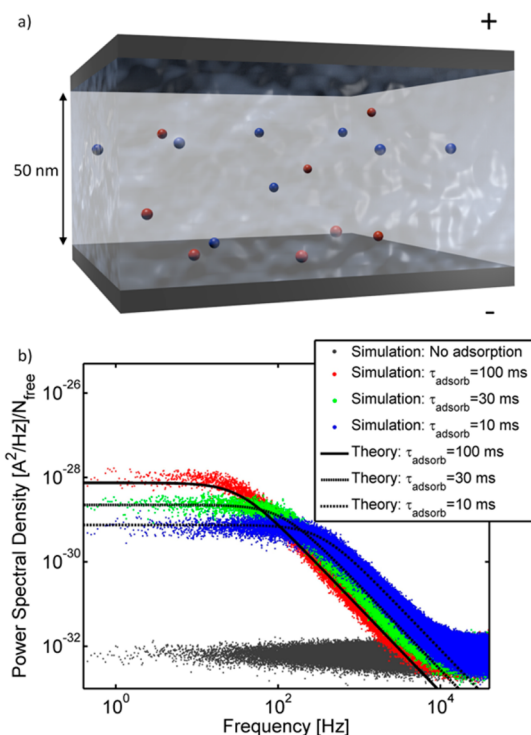


Figure 1. Simulations based on a parallel plate model that is used to investigate the adsorption and shot-like redox cycling noise separately from number fluctuation noise. (a) Illustration of the geometry. (b) Simulated power spectral densities in comparison to the analytical model. Different colors represent different average adsorption times. The power spectral density is normalized to a single free molecule. The simulations assume a diffusion coefficient of $D = 10^{-9} \text{ m}^2/\text{s}$. All further parameters can be found in the Supporting Material 1.

In the case of adsorbing electrodes, graphs are calculated for different average adsorption times τ_a while the ratio between adsorbed and desorbed molecules remains constant. Spectra are further normalized to a single free molecule present between the electrodes. For the adsorption-free case, we obtain the expected white spectrum of shot-like redox cycling noise that was previously described.³⁴ With an increase in τ_a , however, we find a growing plateau in the low-frequency regime that extends up to a transition frequency f_{trans} . This transition frequency decreases with an increase in τ_a . Above f_{trans} , there is a decrease of the power spectral density according to $1/f^2$ until a second transition frequency, above which the spectra are again dominated by shot-like redox cycling noise. Overall, we find a close agreement between the simulated power spectra (after subtraction of the shot-like redox cycling noise) and the analytical solution.

Modeling Nanofluidic Redox Cycling Sensors. To validate the presented simulation model, we compare the simulation results to experimental data. In a previous study,³⁴ our simulation did not consider any adsorption effects and we had to analytically compensate for the impact of adsorption by processing the simulation data according to Singh *et al.*³³ This required a

rescaling of the frequency axis to model the shift in the effective diffusion constant. In contrast, we now demonstrate that our simulation framework is capable of modeling the full sensor response solely based on adsorption modeled at the molecular level. This enables the application of our simulations to arbitrary designs and also allows modeling noise effects that result from molecular properties. The latter aspect further allows deriving molecular properties from noise spectra, as we will show below.

For the experiments, we used the nanofluidic redox cycling device specified in the Experimental Methods. Since the sensor exhibits symmetry with respect to the longitudinal cross section, we model half of the device at doubled analyte concentration to increase computational efficiency, as shown in Figure 2a.

Figure 2b presents simulated data for the case of no adsorption and compares it to experimental data. We can find that the spectra feature a similar shape that results from the geometry of the access channels of the device and the dead volume aside the channel, in which the electrodes do not overlap. However, the simulated spectrum appears to be shifted to higher frequencies. This result is in line with our expectations, since adsorption is not considered in the simulation and the lateral diffusion constant along the channel therefore exceeds the effective diffusion constant that is observed in the experiment.

In order to address this issue, we first calculate the ratio between free and adsorbed molecules from the average current and the standard deviation of the experimentally recorded trace.³¹ Hereby, we first compute the number of free molecules (n_{free}) between the electrodes from the average redox cycling current (I_{rc})²³ and use this value to calculate the average number of adsorbed molecules (n_{ads}) as follows:³¹

$$n_{\text{ads}} = \frac{\langle I_{\text{rc}} \rangle^2}{I_{\text{rc}, \text{std}}^2} - n_{\text{free}} \quad (2)$$

The ratio between adsorbed and desorbed molecules then equals the ratio between the average adsorbed and desorbed times. Therefore we can calculate that the ratio τ_a/τ_d during the experiment was 3.37, whereas the absolute values still remain unknown. Figure 2c shows the simulated spectra for different average adsorption times, with the ratio between adsorbed and desorbed molecules inside the channel is set to the formerly determined experimental conditions. In the plot, we find that the transition frequency (f_{trans}) decreases with an increase in the average adsorption time (τ_a), while the height of the plateau that spreads up to f_{trans} increases with τ_a . At an adsorption time of $\tau_a = 50 \mu\text{s}$, the adsorption noise is dominated by the fluctuation noise of the sensor and cannot be seen any more in the spectra below 150 Hz. In this case, the simulated spectrum closely matches the experimental

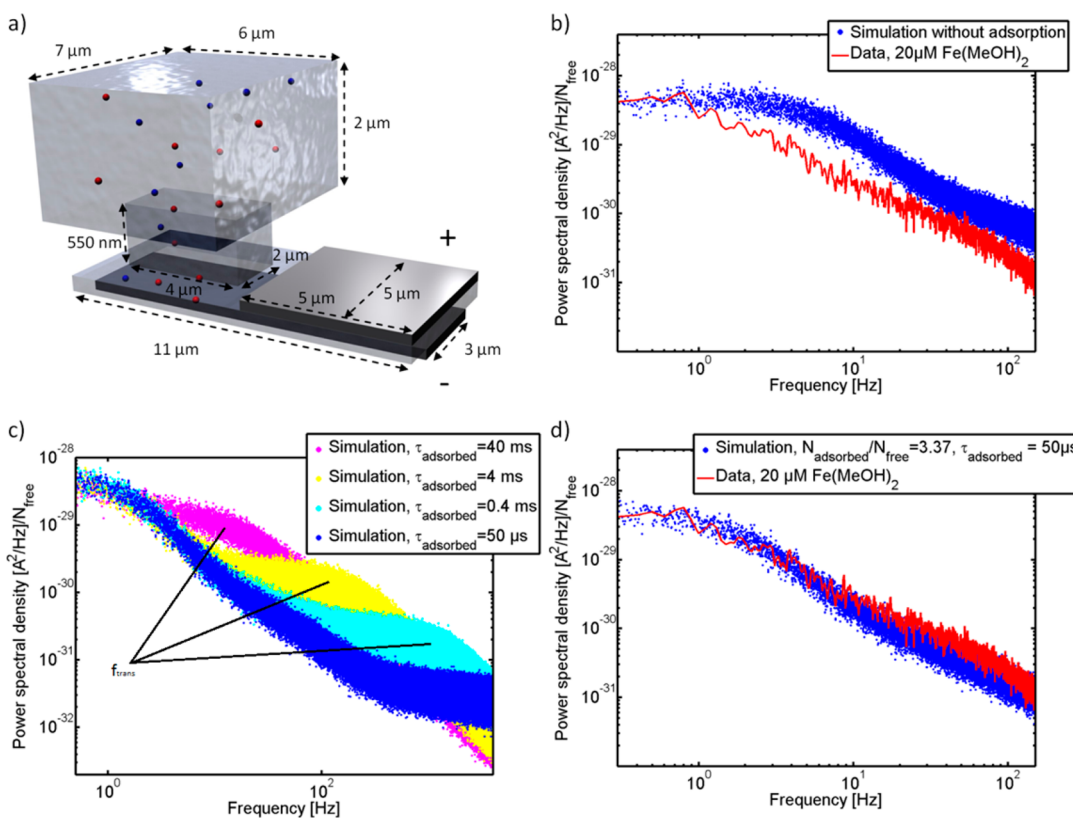


Figure 2. Comparison between simulation and experiment. (a) Illustration of the simulated design. Attached to the access channel on the upper right, a cubic bulk reservoir is added to mimic a bulk reservoir. Dimensions are not to scale. (b) Comparison between experimental data and a simulation that does not consider adsorption effects. (c) Simulations employing different average adsorption times. The ratio between the average adsorbed and desorbed time is held constant to match the experimentally obtained value of 3.37. (d) Comparison between an experimentally obtained current trace and a simulated trace that features an average adsorption time below 200 μ s. The simulations are based on a diffusion coefficient of $D = 6.7 \times 10^{-10}$ m²/s. Further simulation parameters are given in Supporting Material 1.

data, which allows us to draw first conclusions regarding τ_a : since the adsorption plateau cannot be seen in the experiment, we can find an upper limit for the adsorption time (τ_a^{\max}) that is given at the adsorption time τ_a at which the adsorption plateau first disappears within the bandwidth of the experimentally determined spectrum. The spectrum is then only affected through the impact of adsorption on the fluctuation noise. By this means, we find that the average adsorption time in this experiment is smaller than 200 μ s.

Figure 2d presents the experimentally obtained current trace in comparison to a simulated trace that uses a short average adsorption time of 50 μ s. In the plot it can be seen that now both power spectra are in close agreement.

Noise Spectra of SECM Experiments and IDAs. Having shown that our simulation can reproduce experimental measurements, we take a step further and apply our model to other sensor designs. Since all effects are implemented on the molecular level and no further postprocessing of the simulated data is required, we are not limited to idealized systems but may predict noise spectra of nanoscaled redox cycling sensors with almost arbitrary geometry. For this work, we choose

two common designs: an interdigitated array and a scanning electrochemical microscope tip above a conducting surface; see Figure 3a and b. We find that both designs are particularly interesting for determination of average adhesion times in the millisecond range.

The noise spectra of a simulated IDE are given in Figure 3c, where differently colored graphs indicate different average adsorption times. In contrast to the nanofluidic sensors discussed above, the spectra of the IDE do not exhibit any impact of adsorption above a transition frequency of 10 Hz. However, noise levels at low frequencies significantly depend on the simulated adsorption parameters. In the case of no adsorption, we find a flat plateau that spreads up to \sim 40 Hz, but with increasing adsorption times, the noise below 10 Hz increases with adsorption. Accordingly, this section of the spectra can be used to determine the adsorption characteristics of molecules that typically adsorb longer than 10 ms. The data below 10 Hz hereby serve as a direct measure for the average residence time, while the higher frequency components can be used as a calibration of the model.

We additionally simulated the adsorption noise expected in an SECM experiment, as shown in

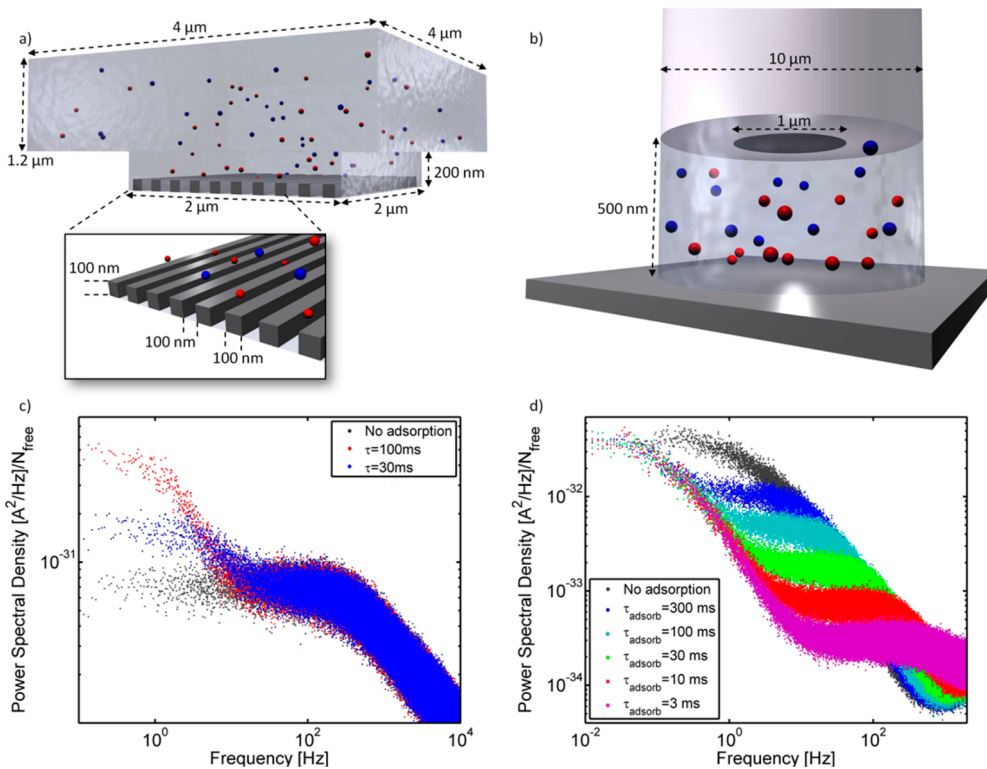


Figure 3. Simulations of other designs. (a and b) Illustrations of the simulated designs of an IDE and an SECM tip. Dimensions are not to scale. (c) Simulated noise spectrum of an IDE for different adsorption times. (d) Simulated noise spectrum of a SECM probe for different adsorption times. All spectra are normalized to a single free molecule. For the simulations, a diffusion coefficient of $D = 10^{-9} \text{ m}^2/\text{s}$ is assumed.

Figure 3d. The spectra show an impact in a wide adsorption regime of average residence times between 3 and 300 ms. In comparison to the spectra of a nonadsorbing sensor, adsorption here induces an additional plateau between 1 and 300 Hz that shifts to higher frequencies and lower amplitudes with an increase in average residence time. Similar to the above specified spectroscopy method based on an IDE, one can utilize this plateau to identify the adsorption characteristics of the analyte under investigation. Thus, we predict that adsorption phenomena on this time scale should become apparent in SECM experiments and hope that in the future our simulations can be confirmed experimentally by the SECM community.

CONCLUSIONS

In conclusion, we introduce a computational framework for the modeling of adsorption effects in

nanoscaled electrochemical sensors. Adsorption is hereby implemented through a model based on fixed adsorption and desorption probabilities at electrodes while each analyte molecule is simulated individually. This approach elucidates the impact of specific molecular adsorption phenomena on the resulting sensor response. A distinct advantage over simplifying analytical concepts is further given by the applicability to almost arbitrary designs. In this work, we first demonstrate that our simulations closely match experimentally obtained data sets and place quantitative limits on the analytes' adsorption properties. Having shown this, we proceed and predict adsorption-dependent noise spectra of IDEs and SECM tips. We further suggest certain features in the noise spectra to be used as key indicators in methods of adsorption spectroscopy. We share our simulation code with other researchers and look forward to seeing it used for different applications.

METHODS

Simulation Framework. We employ an approach that is based on a previously described computational framework.³⁴ In short, the Brownian motion of redox-active molecules is modeled through individual random walks, while molecular trajectories are reflected upon collisions with boundaries. Redox-active molecules can further adopt two oxidation states and participate in redox reactions whenever they come in contact with an appropriately biased electrode. In the simulation, analyte

molecules feature equal diffusion coefficients in both oxidation states. Since we investigate noise in the low-frequency regime, different diffusion coefficients affect only the value of the current obtained per molecule that is located between the electrodes and do not impact the analyzed noise characteristics. A detailed study on the impact of unequal diffusion coefficients was published previously.³⁵

In this work, we expand this simulation by a model of adsorption: in the employed random walk model, molecules

can adsorb in collisions at electrode surfaces with a fixed probability p_a . Hence, a linear adsorption isotherm is assumed, for which the ratio of surface concentration and bulk concentration is always constant. A detailed analysis of the dependency of the adsorption of different redox species on experimental conditions can be found in a previously published study.³⁶ We discuss the exact meaning of p_a below. In experiments, the mean free path of a diffusing molecule is much smaller than the maximal resolution employed computers can model in a reasonable time. Therefore, p_a has to be considered as the average molecular adsorption probability within the temporal random walk step width dt , while the respective molecule is located in a cubic space at the electrode that features an edge length dx equaling the one-dimensional step width of the random walk. The resulting adsorption rate k_a is therefore a function of the random walk step width and p_a . Since the random walk resolution is usually limited by the computational power of computers employed, p_a can be adjusted to match realistic reaction rates. At a given step width, p_a can then be calculated from the desired reaction rate k_a as

$$k_a = \frac{p_a}{2} \frac{dx}{dt} \leftrightarrow p_a = 2k_a \frac{dt}{dx} \quad (3)$$

The product $k_a c_{\text{bulk}} A$ then provides the rate of the absolute number of adsorbing molecules, where c_{bulk} is the bulk concentration of molecules and A the electrode surface. After each temporal step of the random walk, adsorbed molecules can desorb again with the probability p_d . The distribution of the molecules' residence times then follows the geometrical distribution: the probability of detachment after the n th step for $n > 1$ is given by $p_{\text{detach}}(n) = (1 - p_d)^{n-1} p_d$. It features an average residence time τ_a of

$$\tau_a = \frac{dt}{p_d} \quad (4)$$

where dt represents the temporal step width of the random walk. This approach resembles the common model of an adsorbed molecule that oscillates due to its thermal energy and hits an energy barrier at the frequency of its oscillations. However, due to the available computing capacity, dt has to be chosen to be significantly higher. Therefore, p_d represents the total desorption probability of all desorption attempts a molecule performs within dt , while the resulting desorption rate is again linked to the random walk parameters. In order to derive this reaction rate, we have to consider the discrete nature of the random walk, which does not allow surface concentrations but limits the analysis to volume concentrations. The volume concentration at the electrode surface therefore has to be converted into a surface concentration by division through dx . The rate of desorption is then given by

$$k_d = \frac{1}{\tau_d} = \frac{p_d}{dt} \quad (5)$$

Here, the product $k_d c_{\text{surface}} A$ provides the rate of the absolute number of molecules being released, where c_{surface} is the surface concentration.

In most redox cycling experiments, the average adsorption and desorption times are unknown. However, if the employed device features two fully overlapping parallel electrodes that are separated by the distance h , this ratio can be calculated from the currents' variance.³³ For this reason, we also provide the ratio of adsorption and desorption times as a function of the simulation parameters. If we combine eqs 3 and 5, we obtain

$$\frac{\tau_a}{\tau_d} = \frac{p_a}{p_d} \frac{dx}{h} \quad (6)$$

In all simulations, the lateral step width of the random walk is chosen significantly smaller than the smallest design features. The power spectral densities were calculated from the square of the absolute value of the Fourier transform of the simulated current traces and averaged over 10 spectra.

Experimental Methods. Devices were fabricated as reported previously.^{37,38} In short, Pt electrodes as well as a sacrificial Cr layer defining the nanochannel were consecutively deposited

on an oxidized silicon wafer by electron-beam evaporation and patterned by photolithography and lift-off processes. Afterward, the structure was buried in Si_3N_4 and access channels were dry-etched into this passivating layer. The nanochannel was released directly before the experiment by wet etching the sacrificial layer (chromium etchant solution, Selectipur, BASF), and electrode surfaces were subsequently cleaned with 0.5 M H_2SO_4 (Sigma-Aldrich). The device features a nanofluidic channel of $10 \mu\text{m}$ length, $5 \mu\text{m}$ width, and 60 nm height. The channel has access to the bulk reservoir via two $2 \times 4 \mu\text{m}^2$ wide access channels in the passivation layer. The electrodes inside the nanochannel overlap in an area of $30 \mu\text{m}^2$.

In the measurement, the nanofluidic device was connected to a reservoir enclosed in polydimethylsiloxane. The reservoir was filled with the analyte solution, in which a Ag/AgCl reference electrode was immersed. Both top and bottom electrodes were connected to LabVIEW-controlled Femto DDP-CA-300 transimpedance amplifiers used as current meters as well as voltage sources operating at potentials of 450 and 50 mV for the top and bottom electrode, respectively. The analyte, 1,1-ferrocene dimethanol, $\text{Fc}(\text{MeOH})_2$, was acquired from Sigma-Aldrich and prepared in a $20 \mu\text{M}$ solution in Milli-Q water using 1 M KCl (Sigma-Aldrich) as background electrolyte. Ten-second-long current-time traces were recorded at a 150 Hz bandwidth and a 1000 Hz acquisition rate.

Conflict of Interest: The authors declare no competing financial interest.

Acknowledgment. We gratefully acknowledge funding by the Helmholtz Young Investigators Program, The Netherlands Organization for Scientific Research (NWO), and European Research Council (ERC).

Supporting Information Available: Detailed parameters of all simulations (Supporting Material 1). Simulation source code including installation instructions (Supporting Material 2a–f). This material is available free of charge via the Internet at <http://pubs.acs.org>.

REFERENCES AND NOTES

- Watkins, J. J.; Chen, J. Y.; White, H. S.; Abruna, H. D.; Maisonhaute, E.; Amatore, C. Zeptomole Voltammetric Detection and Electron-Transfer Rate Measurements Using Platinum Electrodes of Nanometer Dimensions. *Anal. Chem.* **2003**, *75*, 3962–3971.
- Phillips, P. E. M.; Stuber, G. D.; Heien, M.; Wightman, R. M.; Carelli, R. M. Subsecond Dopamine Release Promotes Cocaine Seeking. *Nature* **2003**, *422*, 614–618.
- Rassaei, L.; Singh, P. S.; Lemay, S. G. Lithography-Based Nanoelectrochemistry. *Anal. Chem.* **2011**, *83*, 3974–3980.
- Kätelhön, E.; Wolfrum, B. On-Chip Redox Cycling Techniques for Electrochemical Detection. *Rev. Anal. Chem.* **2012**, *31*, 7–14.
- Bard, A.; Fan, F.; Kwak, J.; Lev, O. Scanning Electrochemical Microscopy - Introduction and Principles. *Anal. Chem.* **1989**, *61*, 132–138.
- Kwak, J.; Bard, A. J. Scanning Electrochemical Microscopy. Apparatus and Two-Dimensional Scans of Conductive and Insulating Substrates. *Anal. Chem.* **1989**, *61*, 1794–1799.
- Shao, Y. H.; Mirkin, M. V.; Fish, G.; Kokotov, S.; Palanker, D.; Lewis, A. Nanometer-Sized Electrochemical Sensors. *Anal. Chem.* **1997**, *69*, 1627–1634.
- Wittstock, G.; Schuhmann, W. Formation and Imaging of Microscopic Enzymatically Active Spots on an Alkanethiolate-Covered Gold Electrode by Scanning Electrochemical Microscopy. *Anal. Chem.* **1997**, *69*, 5059–5066.
- Macpherson, J. V.; Unwin, P. R. Combined Scanning Electrochemical-Atomic Force Microscopy. *Anal. Chem.* **2000**, *72*, 276–285.
- Fernandez, J. L.; Walsh, D. A.; Bard, A. J. Thermodynamic Guidelines for the Design of Bimetallic Catalysts for Oxygen Electrocatalysis and Rapid Screening by Scanning Electrochemical Microscopy. M-Co (M: Pd, Ag, Au). *J. Am. Chem. Soc.* **2005**, *127*, 357–365.

11. Sanderson, D. G.; Anderson, L. B. Filar Electrodes: Steady-State Currents and Spectroelectrochemistry at Twin Interdigitated Electrodes. *Anal. Chem.* **1985**, *57*, 2388–2393.
12. Chidsey, C. E.; Feldman, B. J.; Lundgren, C.; Murray, R. W. Micrometer-Spaced Platinum Interdigitated Array Electrode: Fabrication, Theory, and Initial Use. *Anal. Chem.* **1986**, *58*, 601–607.
13. Morita, M.; Niwa, O.; Horiuchi, T. Interdigitated Array Microelectrodes as Electrochemical Sensors. *Electrochim. Acta* **1997**, *42*, 3177–3183.
14. Dam, V. A. T.; Olthuis, W.; van den Berg, A. Redox Cycling with Facing Interdigitated Array Electrodes as a Method for Selective Detection of Redox Species. *Analyst* **2007**, *132*, 365–370.
15. Aoki, A.; Matsue, T.; Uchida, I. Electrochemical Response at Microarray Electrodes in Flowing Streams and Determination of Catecholamines. *Anal. Chem.* **1990**, *62*, 2206–2210.
16. Niwa, O.; Xu, Y.; Halsall, H.; Heineman, W. Small-Volume Voltammetric Detection of 4-Aminophenol with Interdigitated Array Electrodes and Its Application to Electrochemical Enzyme-Immunoassay. *Anal. Chem.* **1993**, *65*, 1559–1563.
17. Goluch, E.; Wolfrum, B.; Singh, P.; Zevenbergen, M.; Lemay, S. Redox Cycling in Nanofluidic Channels Using Interdigitated Electrodes. *Anal. Bioanal. Chem.* **2009**, *394*, 447–456.
18. Ino, K.; Saito, W.; Koide, M.; Umemura, T.; Shiku, H.; Matsue, T. Addressable Electrode Array Device with IDA Electrodes for High-Throughput Detection. *Lab Chip* **2011**, *11*, 385.
19. Henry, C. S.; Fritsch, I. Microcavities Containing Individually Addressable Recessed Microdisk and Tubular Nanoband Electrodes. *J. Electrochem. Soc.* **1999**, *146*, 3367–3373.
20. Neugebauer, S.; Müller, U.; Lohmüller, T.; Spatz, J. P.; Stelzle, M.; Schuhmann, W. Characterization of Nanopore Electrode Structures as Basis for Amplified Electrochemical Assays. *Electroanalysis* **2006**, *18*, 1929–1936.
21. Lohmüller, T.; Müller, U.; Breisch, S.; Nisch, W.; Rudorf, R.; Schuhmann, W.; Neugebauer, S.; Kaczor, M.; Linke, S.; Lechner, S.; et al. Nano-Porous Electrode Systems by Colloidal Lithography for Sensitive Electrochemical Detection: Fabrication Technology and Properties. *J. Micromech. Microeng.* **2008**, *18*, 115011.
22. Ma, C.; Contento, N. M.; Gibson, L. R.; Bohn, P. W. Recessed Ring–Disk Nanoelectrode Arrays Integrated in Nanofluidic Structures for Selective Electrochemical Detection. *Anal. Chem.* **2013**, *85*, 9882–9888.
23. Ma, C.; Contento, N. M.; Gibson, L. R.; Bohn, P. W. Redox Cycling in Nanoscale-Recessed Ring-Disk Electrode Arrays for Enhanced Electrochemical Sensitivity. *ACS Nano* **2013**, *7*, 5483–5490.
24. Hüskes, M.; Stockmann, R.; Offenhausser, A.; Wolfrum, B. Redox Cycling in Nanoporous Electrochemical Devices. *Nanoscale* **2014**, *6*, 589–598.
25. Wolfrum, B.; Zevenbergen, M.; Lemay, S. Nanofluidic Redox Cycling Amplification for the Selective Detection of Catechol. *Anal. Chem.* **2008**, *80*, 972–977.
26. Kätelhön, E.; Hofmann, B.; Lemay, S. G.; Zevenbergen, M. A. G.; Offenhausser, A.; Wolfrum, B. Nanocavity Redox Cycling Sensors for the Detection of Dopamine Fluctuations in Microfluidic Gradients. *Anal. Chem.* **2010**, *82*, 8502–8509.
27. Fan, F.-R. F.; Bard, A. J. Electrochemical Detection of Single Molecules. *Science* **1995**, *267*, 871–874.
28. Fan, F.-R. F.; Bard, A. J. An Electrochemical Coulomb Staircase: Detection of Single Electron-Transfer Events at Nanometer Electrodes. *Science* **1997**, *277*, 1791–1793.
29. Zevenbergen, M. A. G.; Singh, P. S.; Goluch, E. D.; Wolfrum, B. L.; Lemay, S. G. Stochastic Sensing of Single Molecules in a Nanofluidic Electrochemical Device. *Nano Lett.* **2011**, *11*, 2881–2886.
30. Singh, P. S.; Kätelhön, E.; Mathwig, K.; Wolfrum, B.; Lemay, S. G. Stochasticity in Single-Molecule Nanoelectrochemistry: Origins, Consequences, and Solutions. *ACS Nano* **2012**, *6*, 9662–9671.
31. Lemay, S. G.; Kang, S.; Mathwig, K.; Singh, P. S. Single-Molecule Electrochemistry: Present Status and Outlook. *Acc. Chem. Res.* **2013**, *46*, 369–377.
32. Zevenbergen, M. A. G.; Singh, P. S.; Goluch, E. D.; Wolfrum, B. L.; Lemay, S. G. Electrochemical Correlation Spectroscopy in Nanofluidic Cavities. *Anal. Chem.* **2009**, *81*, 8203–8212.
33. Singh, P. S.; Chan, H.-S. M.; Kang, S.; Lemay, S. G. Stochastic Amperometric Fluctuations as a Probe for Dynamic Adsorption in Nanofluidic Electrochemical Systems. *J. Am. Chem. Soc.* **2011**, *133*, 18289–18295.
34. Kätelhön, E.; Krause, K. J.; Singh, P. S.; Lemay, S. G.; Wolfrum, B. Noise Characteristics of Nanoscaled Redox-Cycling Sensors: Investigations Based on Random Walks. *J. Am. Chem. Soc.* **2013**, *135*, 8874–8881.
35. Mampallil, D.; Mathwig, K.; Kang, S.; Lemay, S. G. Redox Couples with Unequal Diffusion Coefficients: Effect on Redox Cycling. *Anal. Chem.* **2013**, *85*, 6053–6058.
36. Mampallil, D.; Mathwig, K.; Kang, S.; Lemay, S. G. Reversible Adsorption of Outer-Sphere Redox Molecules at Pt Electrodes. *J. Phys. Chem. Lett.* **2014**, *5*, 636–640.
37. Mathwig, K.; Lemay, S. Pushing the Limits of Electrical Detection of Ultralow Flows in Nanofluidic Channels. *Micromachines* **2013**, *4*, 138–148.
38. Mathwig, K.; Mampallil, D.; Kang, S.; Lemay, S. G. Electrical Cross-Correlation Spectroscopy: Measuring Picoliter-Per-Minute Flows in Nanochannels. *Phys. Rev. Lett.* **2012**, *109*, 118302.
39. Zevenbergen, M. A. G.; Krapf, D.; Zuidam, M. R.; Lemay, S. G. Mesoscopic Concentration Fluctuations in a Fluidic Nanocavity Detected by Redox Cycling. *Nano Lett.* **2007**, *7*, 384–388.